



**HAL**  
open science

## Elasticity and viscosity of BaO-TiO<sub>2</sub>-SiO<sub>2</sub> glasses in the 0.9 to 1.2T(g) temperature interval

Pierre Mezeix, Fabrice Célarié, Patrick Houizot, Yann Gueguen, Francisco Munoz, Tanguy Rouxel

### ► To cite this version:

Pierre Mezeix, Fabrice Célarié, Patrick Houizot, Yann Gueguen, Francisco Munoz, et al.. Elasticity and viscosity of BaO-TiO<sub>2</sub>-SiO<sub>2</sub> glasses in the 0.9 to 1.2T(g) temperature interval. *Journal of Non-Crystalline Solids*, 2016, 445-446, pp.45-52. 10.1016/j.jnoncrysol.2016.05.006 . hal-01395442

**HAL Id: hal-01395442**

**<https://univ-rennes.hal.science/hal-01395442v1>**

Submitted on 17 Feb 2017

**HAL** is a multi-disciplinary open access archive for the deposit and dissemination of scientific research documents, whether they are published or not. The documents may come from teaching and research institutions in France or abroad, or from public or private research centers.

L'archive ouverte pluridisciplinaire **HAL**, est destinée au dépôt et à la diffusion de documents scientifiques de niveau recherche, publiés ou non, émanant des établissements d'enseignement et de recherche français ou étrangers, des laboratoires publics ou privés.

## Elasticity and viscosity of BaO-TiO<sub>2</sub>-SiO<sub>2</sub> glasses in the 0.9 to 1.2T<sub>g</sub> temperature interval

P. Mezeix<sup>1,§</sup>, F. Célarié<sup>1</sup>, P. Houizot<sup>1</sup>, Y. Gueguen<sup>1</sup>, F. Muñoz<sup>2</sup>, and T. Rouxel<sup>1§</sup>

<sup>1</sup>Département "Mécanique et Verre", Institut de Physique de Rennes, UMR UR1-CNRS 6251,  
Campus de Beaulieu, 35042 Rennes cedex

<sup>2</sup>Instituto de Cerámica y Vidrio (CSIC), Kelsen 5, 28049 Madrid, Spain

**Abstract:** In spite of the potential applications of glasses in the BaO-TiO<sub>2</sub>-SiO<sub>2</sub> (BTS) system, the mechanical properties of these glasses were little studied so far. Several centimeters large batches of glasses along the 0.3BaO- $x$ TiO<sub>2</sub>-(0.7- $x$ )SiO<sub>2</sub> composition line were prepared. Their creep behavior and elastic moduli were investigated as a function of  $x$  (from  $x = 0$  to  $x = 0.3$ ). Titanium increases the atomic packing density as well as the volume density of energy and so do the elastic moduli. An excellent agreement is found between the elastic softening index ( $\alpha$ ) and the liquid fragility ( $m$ ) (according to Angell's concept [1]). Nevertheless, as TiO<sub>2</sub> is added the glass-forming liquid becomes more "fragile". The explanation might lie in the structural similarity between the fresnoite crystal and the glass structure consisting of island-like Si-Ti rich units surrounded by barium-rich channels. These islands would contribute to the increase in rigidity whereas the Ba-rich channels, acting as a lubricant, would make the viscous flow more temperature sensitive.

Key words: Viscosity, elasticity, glass, fresnoite, creep

§: corresponding authors: [pierre.mezeix@univ-rennes1.fr](mailto:pierre.mezeix@univ-rennes1.fr) ; [tanguy.rouxel@univ-rennes1.fr](mailto:tanguy.rouxel@univ-rennes1.fr)

## 1. Introduction

The most widely used materials for piezoelectric actuators, transducers, thermal switches, memory storage devices and sensors are Lead Zirconate Titanate ( $\text{Pb}(\text{Zr,Ti})\text{O}_3$ ) or PZT. Considering the toxicity of lead, there is a great interest in developing environment and human friendly piezoelectric materials [2]. Ceramics were the most promising materials to replace PZT so far, such as  $(\text{K,Na})\text{NbO}_3$ ,  $0.5(\text{BiNa})\text{TiO}_3\text{-BaTiO}_3$  or  $(\text{Ba,Ca})(\text{Zr,Ti})\text{O}_3$  based materials. The  $\text{BaO-TiO}_2\text{-SiO}_2$  (BTS) system has also been widely studied because of the fresnoite crystallized phase ( $\text{Ba}_2\text{TiSi}_2\text{O}_8$ ), which exhibits piezoelectricity [3]. A suitable method to obtain dense and uniform size fresnoite ceramics is to crystallize fresnoite glass.

Many authors have studied fresnoite crystallization kinetics in glasses and fresnoite glass-ceramics properties [4–8] but only few have paid attention to the study of BTS-type glasses outside of the fresnoite stoichiometric composition [9,10]. These glasses exhibit non-linear optical properties and high dielectric constant [11]. In the present study, several glasses were synthesized along the 30 mol.% BaO axis and their elastic moduli ( $E$ ,  $K$ ,  $\mu$ ) and shear viscosity coefficient ( $\eta$ ) were measured as a function of temperature in the  $0.9$  to  $1.2T_g$  interval. The temperature dependence of  $\eta$  is discussed in the light of the elastic softening occurring above  $T_g$ . Preliminary investigations were conducted with Raman scattering and IR-Visible spectroscopies to assess the glass network structure and to identify some correlation to the mechanical behavior.

## 2. Materials and experimental techniques

$0.3\text{BaO-xTiO}_2\text{-(0.7-x)SiO}_2$  glasses with  $x$  between 0 and 0.3 were prepared by melt-quenching with  $\text{BaCO}_3$  (99%),  $\text{TiO}_2$  (99%) and  $\text{SiO}_2$  (99.9%) starting materials from Sigma Aldrich. The powder mixture was introduced in a ball-milling machine for 10 minutes and then melted in a Platinum-Rhodium crucible in an electric furnace at  $1770 - 1800$  K for 2 hours. 50 g batches were quenched in a pre-heated (at 700 K) super alloy (Inconel 600) mold and annealed at  $T_g-10$  K for 5 hours. Glasses were cut and mechanically polished to obtain a mirror surface and parallel geometry. Dense, homogeneous, transparent and colorless ( $x = 0$  to 0.05) to yellowish ( $x = 0.10$  to 0.20) and brownish ( $x = 0.25$  to 0.30) glasses were obtained (Fig. 1). A smaller than 0.5 mol.% difference was found between the nominal composition and the actual one as determined by Energy-Dispersive X-ray Spectroscopy analysis.

Density,  $\rho$ , was measured by Archimedes' method in distilled water with an accuracy of  $0.01 \text{ g/cm}^3$ . For each glass, the density was taken as the average value over 10 measurements with different pieces from the same batch. Differential Thermal Analysis (DTA) was performed using a SDT 2960 TA Instrument. The glass transition temperature,  $T_g$ , was taken as the temperature at which the endothermic effect is observed at  $10 \text{ K}\cdot\text{min}^{-1}$  using a platinum crucible containing  $\sim 50$  mg of bulk glass. The Coefficient of linear Thermal Expansion (CTE) was estimated in the  $500\text{-}800$  K temperature interval from thermal expansion curves obtained using a Thermo-Mechanical Analysis (TMA) 2930 CE apparatus (TA Instrument). Absorption spectra were measured using a Perkin-Elmer Lambda 950 UV-visible spectrometer in the  $300 - 900 \text{ nm}^{-1}$  frequency range. Raman scattering spectroscopy was carried out in the range of  $220\text{-}3800 \text{ cm}^{-1}$  with a Witec Alpha 300RA Raman-AFM confocal spectrometer using a 532 nm laser wavelength excitation, a 39 mW power. Elastic moduli at room temperature were obtained using UltraSonic Echography (USE) by means of 10 MHz piezoelectric transducers in contact with the sample via a coupling gel. Young's modulus,  $E$ , and the shear modulus,  $\mu$ , are given by:

$$E = \rho(3V_l^2 - 4V_t^2)/(V_l^2/V_t^2 - 1) \quad (1)$$

$$\mu = \rho V_t^2 \quad (2)$$

where  $V_l$  and  $V_t$  are respectively the longitudinal and transversal wave speeds.

Then Poisson's ratio ( $\nu$ ) and the bulk modulus ( $K$ ) can be easily calculated:

$$\nu = E/2\mu - 1 \quad (3)$$

$$K = E/[3(1 - 2\nu)] \quad (4)$$

Values for the elastic moduli at room temperature are reported in table 1. Errors are mostly due to the measurements of the sample density and size (which was taken with an accuracy of 50  $\mu\text{m}$ ).

Elastic moduli were obtained as a function of temperature using an impulse excitation technique [12,13]. Rectangular samples were cut from the bulk glasses and were suspended by platinum wires at the position of the nodes for their first bending vibration mode, then placed in an electric furnace. Samples were heated at 10  $\text{K}\cdot\text{min}^{-1}$  up to  $T_g+100$  K. In this method the sample is excited periodically by the impact of a small dense alumina projectile. The vibration signal is captured by a microphone and analyzed using a Resonance Frequency and Damping Analyzer (RFDA). A Fast-Fourier Transformation is then made to extract the resonance frequencies from the signal. The present investigations were limited to the shear modulus, which is given by [14]:

$$\mu = 4LA_m f_t^2 / bt \quad (5)$$

where L is the length, b the width, t the thickness, m the mass of sample,  $f_t$  the main frequency for torsion and A a constant that depends on the geometry of the sample (typically  $A \sim 0.01 - 0.02$ ).

The major source for experimental error lies in the measurement of the sample dimensions (L and t). Temperature was controlled using a thermocouple placed at  $\sim 1$  cm above the sample. Shear modulus values and their temperature dependence are reported in Table 2.

The shear viscosity coefficient ( $\eta$ ) was measured using a creep testing machine equipped with alumina pistons and support and allowing for a differential measurement of the specimen displacement in the hot zone [15,16]. The parallelepipedic sample ( $5 \times 5 \times 8$   $\text{mm}^3$ ) was heated at 5  $\text{K}\cdot\text{min}^{-1}$  to the target temperature and the specimen displacement was recorded as a function of the time during isothermal stages by means of a Linear Variable Differential Transducer (LVDT) sensor by differential measurement between the upper and lower piston. For each temperature step, when the quasi-stationary stage is reached, e.g. the strain rate  $\dot{\epsilon}$  is constant,  $\eta$  (Pa.s) is calculated according to Trouton's law [17]:

$$\eta = \sigma / (3\dot{\epsilon}) \quad (6)$$

where  $\sigma$  (Pa) is the applied stress,  $\sigma = Fh/(S_0h_0)$ , and  $\epsilon$  is the strain,  $\epsilon = \ln(h/h_0)$ .

As far as a constant volume throughout deformation is assumed,  $S = S_0h_0/h$ .  $h$ ,  $h_0$  and  $S_0$  are the height, the initial height and surface of the sample, respectively. The applied load, F, is of 245 N.

### 3. Results and discussion

#### 3.1. Structure and physical properties

The addition of  $\text{TiO}_2$  increases the density in agreement with a rule of mixtures ( $\text{TiO}_2$  and  $\text{SiO}_2$  have densities of 4.23 and 2.65  $\text{g}\cdot\text{cm}^{-3}$ , respectively). Values for  $T_g$  obtained from DTA analysis, RFDA and creep measurements are reported in Table 1. Indeed, the transition range can also be estimated from the creep curves, assuming that  $T_g$  is the temperature at which  $\log_{10}(\eta) = 12$ , and from the high temperature elasticity curves, where the transition range is taken as the intersection between the softening regimes associated with the glassy (solid) state and the liquid states (see § 3.2 for details). In the present case,  $T_g$  values as obtained by means of these different techniques are in good agreement (Table 1). Values obtained from creep experiments are plotted in Fig. 6.  $T_g$  is found to increase linearly with  $\text{TiO}_2$  molar content.

As the content of  $\text{TiO}_2$  increases, the color of the glasses changes from white (transparent) to yellowish, and further to orange and brown-red (Fig. 1). The red-shift and the absorbance increase were characterized by UV-visible absorption (Fig. 2). The absence of a 500 nm band and of a blue color indicates that the amount of  $\text{Ti}^{3+}$ , if any, is very small. The  $\text{Ti}^{4+}\text{-O}^{2-}$  charge transfer band is responsible for the yellowish color of these glasses [18].

The Raman spectrum (Fig. 3) of the titanium free glass exhibits several vibrational bands including a broad one at 553  $\text{cm}^{-1}$ . It also exhibits a weak band at 770  $\text{cm}^{-1}$  that is attributed to the motion of Si atoms against their oxygen cage [19] and two peaks at 939 and 1080  $\text{cm}^{-1}$ . These latter peaks are attributed to the  $Q^2$  and  $Q^3$  Si based tetrahedral units (where n in  $Q^n$  is the number of bridging oxygens per  $\text{SiO}_4$  tetrahedron) respectively [20]. The presently studied glasses have their composition relatively close to the one of the fresnoite crystalline phase ( $\text{Ba}_2\text{TiSi}_2\text{O}_8$ ) and there are

thus clear similarities between our Raman spectra and those reported by the former authors [21–23]. The bands between  $280\text{ cm}^{-1}$  and  $360\text{ cm}^{-1}$  can be interpreted as the translations and bending modes of  $\text{TiO}_5$  and  $\text{Si}_2\text{O}_7$  groups [24]. Indeed, these bands are not observed in barium glasses [23]. The Raman spectra of fresnoite-like glasses show a very intense peak at around  $860\text{ cm}^{-1}$ , corresponding to the stretching mode of Ti-O within  $\text{TiO}_5$  groups, and indicating a very short distance of Ti-O bonds [25]. In this configuration, the apical oxygen is strongly bonded to titanium (forming what can be considered as a double Ti=O bond), and is practically not bonded to the other cations of the structure [22]. This large band is also assimilated to the stretching vibration of Ti-O\* (where O\* stands for NBO) bonds [21]. In the glasses where  $x > 0$ , a similar very intense and broad band appears at around  $870\text{ cm}^{-1}$  and seems to be composed of two large peaks. This broad band seems to be shifted to lower frequency as  $\text{TiO}_2$  is added to the glass, to  $863\text{ cm}^{-1}$  for  $x = 0.30$ . The high frequency vibrational bands for rutile and anatase (where Ti is Ti[VI]) are at  $613$ , and  $638\text{ cm}^{-1}$ , whereas for  $\beta\text{-Ba}_2\text{TiO}_4$  (where Ti is Ti[IV]) it is found at  $767\text{ cm}^{-1}$ . For fresnoite, (where Ti is Ti[V]), the main vibrational band is at  $867\text{ cm}^{-1}$  [23]. The main band in the present glasses is found at  $870\text{ cm}^{-1}$ , indicating a close similarity with the fresnoite crystal, suggesting that Ti is very likely to be mainly in 5-fold coordination, in agreement with previous investigations [20]. When  $x > 0.15$  an intense shoulder appears at around  $670\text{ cm}^{-1}$ . This shoulder could be attributed to the vibration of  $\nu(\text{Si-O-Si})$  mode [23]. This band could also result from the formation of 6-fold coordinated Ti [26]. The fact that this band only shows up in glasses with more than 10 mol.%  $\text{TiO}_2$  would support this latter interpretation. This corresponds to the region in which  $\text{TiO}_2\text{-SiO}_2$  glasses become phase separated [26] suggesting that no Ti[VI] is present in the homogeneous glass region. This is an indication that phase separation may occur when  $x > 0.10$ . The  $1080\text{ cm}^{-1}$  peak which can be found in all these glasses corresponds to the  $Q^3$  and shifts to lower frequency as  $x$  increases, down to  $1040\text{ cm}^{-1}$  for  $x = 0.30$ . This shift in frequency is due to the replacement of Si by Ti in the glass network [24]. This observation indicates a random substitution of Si by Ti within the glass network.

In regard of these structural investigations, considering that Ti is predominantly 5-fold coordinated, and assuming that as in the fresnoite crystalline phase barium is mostly found in the neighborhood of titanium compensating the negative charge of the non-bridging oxygen (one barium can thus bring the electroneutrality to two  $\text{TiO}_5$  units) then the average number of bridging oxygens per Si- and Ti-based structural units can be written:  $N_{\text{BO}} = (4[\text{Si}] - 2([\text{Ba}] - [\text{Ti}]/2) + 4[\text{Ti}])/([\text{Si}] + [\text{Ti}])$ , so that:

$$N_{\text{BO}} = (4[\text{Si}] + 5[\text{Ti}] - 2[\text{Ba}])/([\text{Si}] + [\text{Ti}]) \quad (7)$$

According to the stoichiometry of these glasses, with  $x$  the molar content of titanium oxide:

$$N_{\text{BO}} = (x + 2.2)/0.7 \quad (8)$$

Values for  $N_{\text{BO}}$  range from 3.14 to 3.57 and are indicative of the cross-linking degree (Table 1). These values suggest that the glass network is mainly built on  $Q^3$  units which are expected to be found in a growing number as titania substitutes for silica. According to Raman spectra the Si-based  $Q^3$  units predominate at low  $\text{TiO}_2$  content, but some fraction of  $Q^2$  units is also present, suggesting some disproportionation (a fraction of  $Q^3$  units is supposed to have been replaced by a combination of  $Q^2$  and  $Q^4$  units). The increase of the amount of  $Q^3$  units with  $x$  is consistent with the fact that the number of bridging oxygens per Si-based tetrahedron increases with  $x$  (this number is expressed as  $(2.2 - 3x)/(0.7 - x)$ ). However, the quantification of the  $Q^n$  silicate species from the Raman spectra is out of reach, inasmuch bands are relatively broad and overlapping. For example, the  $Q^2$  band turns out to be absorbed in the broad and intense band at about  $850\text{ cm}^{-1}$  originating from the Ti environment.

$T_g$  and CTE measurements bring some complementary information.  $T_g$  increases with  $x$  but the rate of change drops significantly as  $x$  becomes larger than say  $\sim 0.1$ - $0.15$ . In parallel, the CTE increases sharply from  $8.7 \cdot 10^{-6}\text{ K}^{-1}$  to  $13.4 \cdot 10^{-6}\text{ K}^{-1}$  for  $x$  up to  $\sim 0.1$ - $0.15$  and then decreases monotonically to about  $9.7 \cdot 10^{-6}\text{ K}^{-1}$ . These tendencies suggest that some important structural change takes place at  $x \sim 0.1$ - $0.15$ , that is when the Ba/Ti ratio approaches the one of the fresnoite crystallized phase ( $\text{Ba}_2\text{TiSi}_2\text{O}_8$ ), so that fresnoite-like composition domains might form.

Schematic drawings of the atomic network structures in the case of titanium-free and titanium-rich barium silicate glasses are presented in Fig. 4. Ba-rich channels can be tentatively drawn in a network where silicon and titanium are considered as network formers.

## 3.2. Elasticity

### 3.2.1. At room temperature

Elastic moduli and Poisson's ratio increase monotonically with the TiO<sub>2</sub> content (Fig. 5). The fact that Ti might be in 4, 5- and maybe even in 6-fold coordinated to oxygen makes the ab-initio prediction of the elastic moduli with semi-empirical models such as the one by Makishima et al. [27] quite difficult (the model is found to underestimate the elastic moduli by up to 20%, especially at large TiO<sub>2</sub> content, (Fig. 5)). Alternatively, trends in bulk modulus can be assessed by investigating the volume density of energy, simply extending the 1<sup>st</sup> Grüneisen rule to oxide mixtures [28]:

$$K = mnU_0/(9V_0) \quad (9)$$

where  $U_0$  is a molar energy,  $V_0$  is a molar volume at equilibrium and  $m$  and  $n$  are the exponents of the power law (Lennard-Jones type) describing respectively the attractive and the repulsive terms of interatomic potential.

For a multi-component glass, this volume density of energy can be estimated from both density of the glass and from thermochemistry data for each constituent, respectively:

$$\langle U_0 \rangle / \langle V_0 \rangle = (\sum f_i \Delta H_{ai}) / (\sum f_i M_i / \rho_{\text{glass}}) \quad (10)$$

where  $\rho_{\text{glass}}$  is the density of the glass, and  $f_i$ ,  $M_i$  and  $\Delta H_{ai}$  are the molar fraction, the molar mass, and the dissociation enthalpy of the  $i^{\text{th}}$  constituent respectively. For the  $i^{\text{th}}$  constituent written as  $A_x B_y$ , according to an ordinary Born-Haber cycle:

$$\Delta H_{ai} = x\Delta H_f^0(A,g) + y\Delta H_f^0(B,g) - \Delta H_f^0(A_x B_y) \quad (11)$$

where  $\Delta H_f^0(A,g)$  and  $\Delta H_f^0(B,g)$  are the atomization (sublimation) enthalpies of cations (A) and (B) respectively and  $\Delta H_f^0(A_x B_y)$  is the standard enthalpy of formation of  $A_x B_y$  compound. The standard formation enthalpy of a cation is equal to its sublimation enthalpy whereas for an anion gaseous in its standard state, the molar dissociation energy of the gas molecules must be considered. The mean dissociation energy ( $\langle U_0 \rangle$ ) provides an estimation of the overall structural energy content in the material and is mostly found to scale with  $T_g$  (Fig. 6). In case where the glass density is unknown, Eq. (10) can be replaced by the following one, which allows for a fully ab-initio calculation:

$$\langle U_0 \rangle / \langle V_0 \rangle = \sum f_i \Delta H_{ai} / (\sum f_i M_i / \rho_i) \quad (12)$$

where  $\rho_i$  is the density of the  $i^{\text{th}}$  starting constituent (added oxide).

The estimated volume density of energy as calculated by means of Eqs. (10,12) is shown in Fig. 7. The difference observed between both series of data can be attributed to the fact that the atomic packing density is larger in the glass than in the parent oxides, as seen in Fig. 8. The atomic packing density ( $C_g$ ) is defined as

$$C_g = \sum f_i V_i / [(\sum f_i M_i) / \rho_{\text{glass}}] \quad (13)$$

Where  $V_i$  is calculated for a constituent  $A_x B_y$  as:

$$V_i = 4/3\pi N(xr_A^3 + yr_B^3) \quad (14)$$

Where  $r_A$  and  $r_B$  are the ionic radii, taken from [29].

$C_g$  is found to increase rapidly with the  $TiO_2$  content and this is corroborated by the concomitant increase of Poisson's ratio (Fig. 5). Interestingly in Fig. 7, the experimental values for  $K$  are found to increase very significantly with the titanium content, from 46.3 to 70.1 GPa which represents a 51 % increase for 30 mol.% addition of  $TiO_2$ , whereas at the same time,  $\langle U_0 \rangle / \langle V_0 \rangle$  increases only by 6 % (from 65.1  $kJ.cm^{-3}$  for the Ti-free glass to 68.9  $kJ.cm^{-3}$  for the one with 30 mol.%  $TiO_2$ ). It is thus suggested that Ti significantly changes the atomic network structure, beyond what could be anticipated from the energy density or from the characteristics of the constituents. This is especially remarkable since the dissociation energy for  $TiO_2$  ( $\approx 667 kJ.mol^{-1}$ ) is smaller than the one for  $SiO_2$  ( $\approx 800 kJ.mol^{-1}$ ) [30]. This is another evidence for the tightening effect of titanium, in spite of an increase of the glass network cross-linking. At the macroscopic scale, the efficient atomic packing, combined with the existence of relatively weak bonds at barium sites offering a poor resistance to shear, leads to relatively large values for  $\nu$  (0.271 to 0.282) in comparison to amorphous silica (0.17) and soda-lime-silica glasses (0.24), despite a remarkably large cross-linking degree.

### 3.2.2. Temperature dependence of the elastic moduli

The temperature dependence of the elastic moduli below  $T_g$  is illustrated in the case of the shear modulus ( $\mu$ ) in Fig. 10. Note that the actual dimensions of the sample at a given temperature were taken into account in the calculation of  $\mu$  from Eq. (5) using the CTE as obtained by TMA (table 1). In order to comply with the 2<sup>nd</sup> principle of thermodynamics the differentiation of  $\mu$  with respect to  $T$  should tend toward zero on approaching 0 K. A good description of our data was obtained by means of the model proposed by Wachtman [31]:

$$\mu = \mu_{0K} - B \exp(-T_0/T) \quad (15)$$

where  $\mu_{0K}$  is the shear modulus on approaching 0 K and  $B$  and  $T_0$  are constants.

At higher temperature ( $T > T_g$ ) an asymptotic approach to the temperature axis is expected as the resistance a liquid opposes to shear becomes smaller and smaller ( $d\mu/dT$  and  $\mu$  tend toward 0 as  $T$  increases). The temperature dependence of the shear modulus in the liquid range can be nicely modeled by means of a power law equation [32].

$$\mu = \mu_{T_g} (T_g/T)^\alpha \quad (16)$$

where  $\mu_{T_g}$  is the shear modulus at the glass transition temperature as derived by intersecting both expressions corresponding to the glassy (Eq. 15) and liquid ranges (Eq. 16) and  $\alpha$  is a constant which expresses the softening rate and turns out to be correlated to the liquid fragility index "m", as discussed below (See § 3.3).

An example of the curve fitting with Eq. 15 and Eq. 16 is given in Fig. 10. The temperature sensitivity of the studied materials is found to increase with the  $TiO_2$  content, both in the sub- and in the above- $T_g$  ranges, as shown by the increases of  $B$  and  $\alpha$  in Eqs. (15,16) (Table 2). This result is in agreement with the fact that Poisson's ratio increases with  $x$  at room temperature (Fig. 5), which reflects the ease for shear relative to volume change as titanium enters the glass network. Note that  $\alpha \approx 0.07$  for a- $SiO_2$ ,  $\alpha \approx 0.98$  for a standard window soda-lime-silica glass (window glass),  $\alpha$  reaches values greater than 2 for precious metals based metallic glasses and is close to 9 for a-Se [32]. In the present case  $\alpha$  ranges from 1.6 ( $x = 0$ ) to 4.6 ( $x = 0.3$ ). According to these values, the presently studied liquids can be considered as relatively sensitive to temperature changes (short glasses) and classified as "fragile" liquids. The remarkable increase of  $\alpha$  with the  $TiO_2$  content is quite surprising provided titanium is tightening the network and increases the network connectivity. This suggests that some easy-to-shear regions form (structural scale) which governs the high temperature behavior, possibly resembling the barium-rich layers present in the fresnoite structure, as sandwiched between (Ti,Si)-rich regions.

### 3.3. Viscosity

Creep experiments were conducted in compression under a constant load corresponding to an initial stress of 10 MPa for temperatures between 0.9 and 1.2 $T_g$ . Because of the large deformation (exceeding 10%) observed as  $T$  approaches 1.2 $T_g$ , the true strain was calculated according to

$$\varepsilon = \int_{h_0}^h (1/h)dh = \ln(h/h_0) \quad (17)$$

and the true strain rate  $\dot{\varepsilon}$  at a specific temperature is expressed as  $\dot{\varepsilon} = \dot{h}/h$ .

The creep deformation exhibits a transient primary creep stage during which the strain-rate keeps decreasing. The lower the temperature is the longer this transient stage lasts. The viscosity coefficient  $\eta$  is derived from the stationary creep (constant strain rate  $\dot{\varepsilon}$ ) observed once time length is much larger than the time constant  $\tau$  associated with this primary stage. A typical creep curve is illustrated in Fig. 11. The addition of titanium greatly increases the viscosity of the glass (Fig. 12), especially in the lower temperature range, where the addition of 30 mol.%  $TiO_2$  results in an increase of  $\eta$  by three orders of magnitude.  $T_g$  is taken as the temperature for a viscosity of  $10^{12}$  Pa.s and is mostly within 20 K from  $T_g$  as determined from DTA measurements (Table 1).

According to an Arrhenius-type viscosity law, the slope of the tangent line at  $T_g$  on the  $\ln(\eta)$  vs  $1/T$  curve (Fig. 14), allows for the estimation of the activation enthalpy for viscous flow, or heat for flow, ( $\Delta H_a$ ) at  $T_g$  :

$$\Delta H_a = R \partial \ln(\eta) / \partial (1/T) \quad (18)$$

The free activation enthalpy of the flow process can be further derived, assuming that the energy barrier for the viscous flow is essentially elastic in nature (which is a common assumption in the field of "plasticity" and is well accepted in creep science) and thus correlates with the rate at which elastic moduli (and especially  $\mu$ ) change with temperature (see [32] for details):

$$\Delta G_a = \Delta H_a / (1 - \chi) \quad (19)$$

where  $\chi$  can be calculated following the equation:

$$\chi = (T/\mu) \partial \mu / \partial T \quad (20)$$

So that:

$$\chi = -\alpha \mu_{T_g} / \mu (T_g/T)^\alpha \quad (21)$$

Taking advantage of the high temperature elasticity results obtained on the presently studied glasses (parameter  $\alpha$ ), the shear viscosity coefficient is then expressed as [32]:

$$\eta = \eta_0 \exp(\Delta G_a(T_g)(T_g/T)^\alpha / [RT]) \quad (22)$$

The fragility index (Angell [1]) is given by:

$$m = \partial \log_{10}(\eta) / \partial (T_g/T) \quad (23)$$

Values for  $\Delta H_a$ ,  $\Delta G_a$  and  $m$  are reported in Table 2, together with the parameters used to describe the high temperature elastic properties. Values obtained for  $\alpha$  are relatively high ( $1 < \alpha < 5$ ) in comparison to those reported for other inorganic liquids, thus suggesting a rapid degradation of the network cross-linking above  $T_g$  and a low connectivity between structural units especially at large  $TiO_2$  content. This observation from high temperature elasticity data is corroborated by the fragility index estimated from the creep behavior (Fig. 14). In the present case,  $m$  ranges from 43.6 ( $x = 0$ ) to 65.9 ( $x = 0.3$ ). These values are relatively high, approaching those for typical fragile liquids like glycerol, chalcogenide, or fluoride, especially at large titanium content. Again, this increase in fragility

with the  $\text{TiO}_2$  content suggests that titanium favors the formation of easy paths for sliding (between more resistant "islands"), in spite of an increase of the overall stiffness and atomic packing efficiency. The structure of the fresnoite crystal [33] is based on  $\text{TiO}_5$  tetragonal pyramids occupying the corners and the base center of the primitive tetragonal cell. The basal oxygen atoms of these pyramids are shared by Si tetrahedra which form  $\text{Si}_2\text{O}_7$  groups. In such a structure,  $\text{Si}_2\text{O}_7$  and  $\text{TiO}_5$  groups are forming rings parallel to the (001) plane and are separated by barium atoms forming Ba-O bonds. The studied glasses have compositions close to the fresnoite ( $\text{Ba}_2\text{TiSi}_2\text{O}_8$ ) stoichiometry and, in analogy to the fresnoite structure, it is likely that (Ti,Si) rich "islands" form with  $\text{TiO}_5$  groups and  $\text{SiO}_4$  tetrahedral units, separated by BaO-rich channels. These islands are strongly packed and polymerized and would be the source for the large elastic moduli, while the barium-rich channels would tend to weaken the resistance to viscous flow by acting as a lubricant between these "islands". In-depth structural investigations (medium range order) are needed to go further on interpretation and to clarify the viscous flow mechanisms.

#### 4. Conclusion

Transparent glasses along the  $0.3\text{BaO}-x\text{TiO}_2-(0.7-x)\text{SiO}_2$  composition line were synthesized by melt-quenching. Structural investigations suggest that as Ti substitutes for Si in the glass network, the number of bridging oxygen per network former (Si, Ti) increases. Ti is mostly 5-fold coordinated, although some Ti(VI) may be present.  $\text{TiO}_5$  groups support one apical oxygen with a very short Ti-O bond, and barium atoms concentrate in the neighborhood of these Ti-based units, to compensate the charge of the non-bridging oxygen atoms.

Elastic properties and creep behavior were investigated for temperature between 293 K and  $1.2T_g$  as a function of  $x$  (for  $x$  between 0 and 0.3). The specific mass, the atomic packing density, the glass transition temperature, and the elastic moduli increase with the titanium content. However, this enhancement of the properties with titanium is accompanied by a greater sensitivity of the elastic moduli and of the shear viscosity coefficient with temperature: the softening rate ( $\alpha$ ) and the fragility ( $m$ ) increase markedly with the  $\text{TiO}_2$  content.

In analogy to the fresnoite crystal structure, it is suggested that (Ti,Si)-rich "islands" form in the glass with  $\text{TiO}_5$  groups and  $\text{SiO}_4$  units, and Ba-rich channels in-between. These highly cross-linked islands associated with a remarkable overall atomic packing density would explain the relatively high stiffness of these glasses. Ba-rich channels are supposed to provide - in the presence of titanium - easy paths for shearing and sliding and to be thus responsible for a large Poisson's ratio, a rapid softening with temperature, and a fragile-like liquid behavior.

#### Acknowledgments

The European Research Council is gratefully acknowledged for funding these researches through the Advanced Grant 320506 (DAMREG) of the European Research Council. Authors are indebted to Instituto de Cerámica y Vidrio (Madrid, Spain) for the Raman scattering and UV-Visible spectroscopy measurements. We are also indebted to the Glass & Ceramics team at the ISCR (University of Rennes 1) for DSC and dilatometry measurements, and to Hervé Orain and Vincent Burgaud at the Glass Mechanics Department for their assistance in the specimens preparation and in creep testing.

## References

- [1] C.A. Angell, Relaxation in liquids, polymers and plastic crystals — strong/fragile patterns and problems, *J. Non-Cryst. Solids* 131-133 (1991) 13 - 31.
- [2] Y. Saito, H. Takao, T. Tani, T. Nonoyama, K. Takatori, T. Homma, T. Nagaya, M. Nakamura, Lead-free piezoceramics, *Nature* 432 (2004) 84 - 87.
- [3] C. Rüssel, Oriented crystallisation of glass. A review, *J. Non-Cryst. Solids* 219 (1997) 212 - 218.
- [4] A.A. Cabral, V.M. Fokin, E.D. Zanotto, C.R. Chinaglia, Nanocrystallization of fresnoite glass. I. Nucleation and growth kinetics, *J. of Non-Cryst. Solids* 330 (2003) 174 - 186.
- [5] N.J. Bang, H. Cho, Y.S. Yang, The Crystallization Mechanism and Dielectric Property of BaTiO<sub>3</sub> - SiO<sub>2</sub> glass, *J. Kor. Phys. Soc.* 32 (1998) 845 - 849.
- [6] K. Shinozaki, T. Honma, T. Komatsu, Elastic properties and Vickers hardness of optically transparent glass-ceramics with fresnoite Ba<sub>2</sub>TiSi<sub>2</sub>O<sub>8</sub> nanocrystals, *Mater. Res. Bull.* 46 (2011) 922 - 928.
- [7] A.M. Rodrigues, J.M.R. Mercury, V.S. Leal, A.A. Cabral, Isothermal and non-isothermal crystallization of a fresnoite glass, *J. of Non-Cryst. Solids* 362 (2013) 114 - 119.
- [8] M. Zhu, B. Wang, P. Liu, H. Yan, Z. Ding, Preparation and properties of BaTiSi<sub>2</sub>O<sub>7</sub> glass-ceramics, *Opt. Mater.* 23 (2003) 323 - 236.
- [9] J. Kim, S.J. Kim, Y.S. Yang, Dielectric and conduction behavior of xBaTiO<sub>3</sub> (1-x) SiO<sub>2</sub> glasses, *Mater. Sci. Eng. A* 304 – 306 (2001) 487 - 490.
- [10] H. Masai, S. Tsuji, T. Fujiwara, Y. Benino, T. Komatsu, Structure and non-linear optical properties of BaO-TiO<sub>2</sub>-SiO<sub>2</sub> glass containing Ba<sub>2</sub>TiSiO<sub>8</sub> crystal, *J. Non-Cryst. Solids* 353 (2007) 2258 - 2262.
- [11] A.P. Zorin, M.L. Zorina, Some properties and the structure of glass of the system BaO-SiO<sub>2</sub>-TiO<sub>2</sub>, *Neorg. Mater.* Vol. 2 n°10 (1966) 1816 - 1819.
- [12] G. Roebben, B. Bollen, A. Brebels, J. Van Humbeeck, O. Van der Biest, Impulse excitation apparatus to measure resonant frequencies, elastic moduli, and internal friction at room and high temperature, *Rev. Sci. Instrum.* 68 (1997) 4511 - 4515.
- [13] P. Gadaud, X. Milhet, S. Pautrot, Bulk and coated materials shear modulus determination by means of torsional resonant method, *Mater. Sci. Eng. A* 521 – 522 (2009) 303 - 306.
- [14] ASTM international, Standard Test Method for Dynamic Young's Modulus, Shear Modulus, and Poisson's Ratio by Impulse Excitation of Vibration, ASTM E1876 – 01 (2006).
- [15] E.H. Fontana, A versatile parallel-plate viscometer for glass viscosity measurements to 1000 degrees C, *Amer. Cer. Soc. Bull.* 49 (1970) 594 - 597.
- [16] P. Webber, J.A. Savage, Measurement of the viscosity of chalcogenide glasses by a parallel plate technique, *J. Mater. Sci.* 16 (1981) 763 - 766.
- [17] F. Trouton, On the coefficient of viscous traction and its relation to that of viscosity, *Proceedings Roy. Soc. A* 77 (519) (1906) 426 - 440.
- [18] M. Chavoutier, D. Caurant, O. Majérus, R. Boulesteix, P. Loiseau, C. Jousseume, E. Brunet, E. Lecomte, Effect of TiO<sub>2</sub> content on the crystallization and the color of (ZrO<sub>2</sub>,TiO<sub>2</sub>)-doped Li<sub>2</sub>O-Al<sub>2</sub>O<sub>3</sub>-SiO<sub>2</sub> glasses, *J. Non-Cryst. Solids* 384 (2014) 15 - 24.

- [19] P.F. McMillan, A Raman spectroscopic study of glasses in the system CaO-MgO-SiO<sub>2</sub>, *Amer. Miner.* 69 (1984) 645 - 659.
- [20] B.O. Mysen, L.W. Finger, D. Virgo, F.A. Seifert, Curve-fitting of Raman spectra of silicate glasses, *Amer. Min.* 67 (1982) 686 - 695.
- [21] S.A. Markgraf, S.K. Sharma, A.S. Bhalla, Raman study of fresnoite-type materials: Polarized single crystal, crystalline powders, and glasses, *J. Mater. Res.* 8 (1993) 635 - 648.
- [22] S. Stassen, P. Tarte, A. Rulmont, The barium titano-disilicate BaTiSi<sub>2</sub>O<sub>7</sub>: a structural investigation by vibrational spectroscopy and X-ray powder diffraction, *Spectrochimica Acta Part A* 54 (1998) 1423 - 1431.
- [23] G. S. Henderson, M. E. Fleet, The structure of Ti-silicate glasses by micro-Raman spectroscopy, *Can. Min.* 33 (1995) 399 - 408.
- [24] T. H. Kim, Y. S. Kim, Y.J. Jeong, Y.H. Na, H.H. Lim, M.S. Cha, B.K. Ryu, Optical Properties and Structure of BaO-TiO<sub>2</sub>-SiO<sub>2</sub> Glass Ceramics, *J. Kor. Ceram. Soc.* 45 (2008) 821 - 826.
- [25] G. Blasse, Fresnoite (Ba<sub>2</sub>TiSi<sub>2</sub>O<sub>8</sub>): A luminescent compound, *J. Inorg. Chem.* 41 (1978) 639 - 641.
- [26] D. L. Evans, Solid Solution of TiO<sub>2</sub> in SiO<sub>2</sub>, *J. Amer. Cer. Soc.* 53 (1970) 418 - 419.
- [27] A. Makishima, J.D. Mackenzie, Direct calculation of Young's modulus of glass, *J. Non-Cryst. Solids* 12 (1973) 35 - 45.
- [28] C. Zwikker, Grüneisen 1<sup>st</sup> rule, *Phys. Prop. Solid Mater.* (1954) p. 90.
- [29] R.D. Shannon, Revised effective ionic radii and systematic studies of interatomic distances in halides and chalcogenides, *Acta Cryst.*, A32 [5] (1976) 751-767.
- [30] Handbook of Chemistry and Physics, Ed. D. R. Lide, 86th Edition, Pub. Taylor & Francis (2005-2006).
- [31] J.B. Wachtman, W.E. Tefft Jr., D.G. Lam, C.S. Apstein, Exponential Temperature Dependence of Young's Modulus for Several Oxide, *Phys. Rev.* 122 (1961) 1754 - 1759.
- [32] T. Rouxel, Thermodynamics of viscous flow and elasticity of glass forming liquids in the glass transition range, *J. Chem. Phys.* 135 (2011) 184501.
- [33] P.B. Moore, S.J. Louisnathan, The crystal structure of fresnoite, Ba<sub>2</sub>(TiO)Si<sub>2</sub>O<sub>7</sub>, *Zeitschrift für Kristallographie* 130 (1969) 438 - 448.

Table 1. Physical and thermal properties of the studied BTS glasses.  $C_g$ ,  $N_{BO}$  and CTE stand for atomic packing density, number of bridging oxygen atoms per (S,Ti)-based structural entities, and CTE (500-800 K).

TiO <sub>2</sub> (Mol.)	Density ( $\rho$ ) (g.cm <sup>-3</sup> )	$C_g$	$N_{BO}$	CTE (10 <sup>-5</sup> .K <sup>-1</sup> )	$T_{gDTA}$ (K)	$T_{g\eta}$ (K)	$T_{gRFDA}$ (K)	E (GPa)	$\mu$ (GPa)	K (GPa)	$\nu$
Error	$\pm 0.0024$			$\pm 0.0756$	$\pm 4.23$	$\pm 2.74$	$\pm 6.30$	$\pm 0.026$	$\pm 0.023$	$\pm 0.044$	$\pm 0.00201$
0%	3.60	0.562	3.14	0.87	971	976	978	64.7	25.5	46.3	0.271
5%	3.66	0.572	3.15	1.23	982	990	998	67.2	26.4	49.2	0.274
10%	3.75	0.585	3.29	1.34	1008	1002	1012	74.9	29.4	55.7	0.276
15%	3.83	0.598	3.36	1.22	1009	1013	1016	78.6	30.6	60.9	0.278
20%	3.90	0.608	3.43	1.06	1012	1021	1024	81.4	31.7	62.9	0.280
25%	3.93	0.614	3.50	0.97	1016	1024	1027	88.3	34.7	64.9	0.281
30%	4.02	0.627	3.57	0.97	1023	1032	1031	91.3	35.6	70.1	0.282

Table 2. High temperature data.

TiO <sub>2</sub> (Mol.)	High temperature elasticity					Creep measurement							
	$\mu_{OK}$ (GPa)	$\mu_{RT}$ (GPa)	$\mu$ ( $T_{gRFDA}$ ) (GPa)	$d[\mu(Tg^-)]/dT * 10^3$	$d[\mu(Tg^+)]/dT * 10^3$	$T_0$	$B * 10^3$	$\alpha$	$\eta$ ( $T_{gATD}$ ) *10 <sup>-12</sup> (Pa.s)	$\Delta H_a$ ( $T_{g\eta}$ ) (kJ.mol <sup>-1</sup> )	$\Delta G_a$ ( $T_{g\eta}$ ) (kJ.mol <sup>-1</sup> )	$\log_{10}(\eta_0)$	$m$
Error		$\pm 0.205$	$\pm 0.198$	$\pm 0.0572$	$\pm 0.0572$				$< \pm 0.3\%$	$\pm 54.46$	$\pm 23.76$		$\pm 0.88$
0%	25.3	25.4	22.8	-4.4	-32.9	829	5.5	1.60	1.32	811	320	-5.25	43.60
5%	27.2	27.1	24.1	-5.1	-61.6	748	5.8	2.29	2.65	864	284	-2.96	44.32
10%	30.7	30.6	26.9	-5.6	-79.8	617	6.5	3.50	0.36	958	263	-1.77	49.50
15%	31.5	31.5	27.7	-5.6	-107.6	659	6.5	4.22	1.32	1039	202	1.50	53.56
20%	32.9	32.6	28.0	-6.9	-111.5	654	8.2	4.35	2.87	1142	229	0.17	58.96
25%	34.1	34.1	29.3	-6.8	-116.1	767	7.4	4.40	2.30	1232	200	1.68	63.35
30%	37.0	36.8	31.6	-8.8	-142.3	767	9.6	4.60	19.20	1293	195	2.01	65.90



Fig. 1. Comparison of color and transparency of the different glasses, from left to right  $x = 0; 0.05; 0.10; 0.15; 0.20; 0.25; 0.30$  (25 mm diameter and 2 mm thick disks).

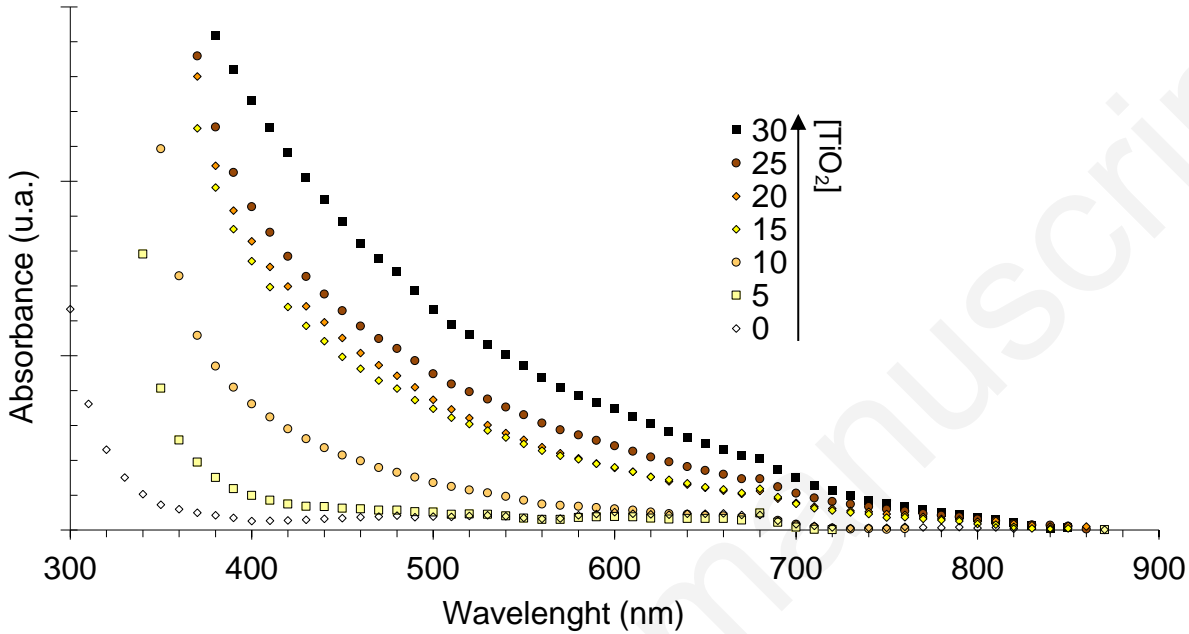


Fig. 2. Absorption spectra for different values of  $x = [TiO_2]$ .

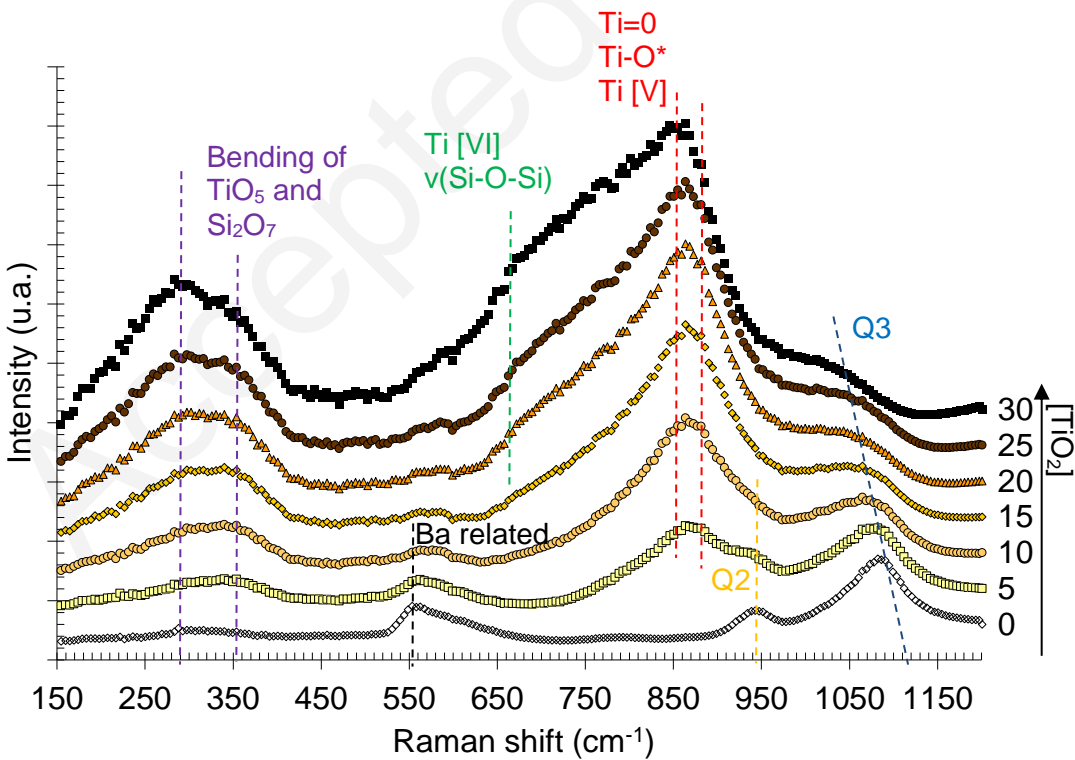


Fig. 3. Raman spectrum for different values of  $x = [TiO_2]$ .

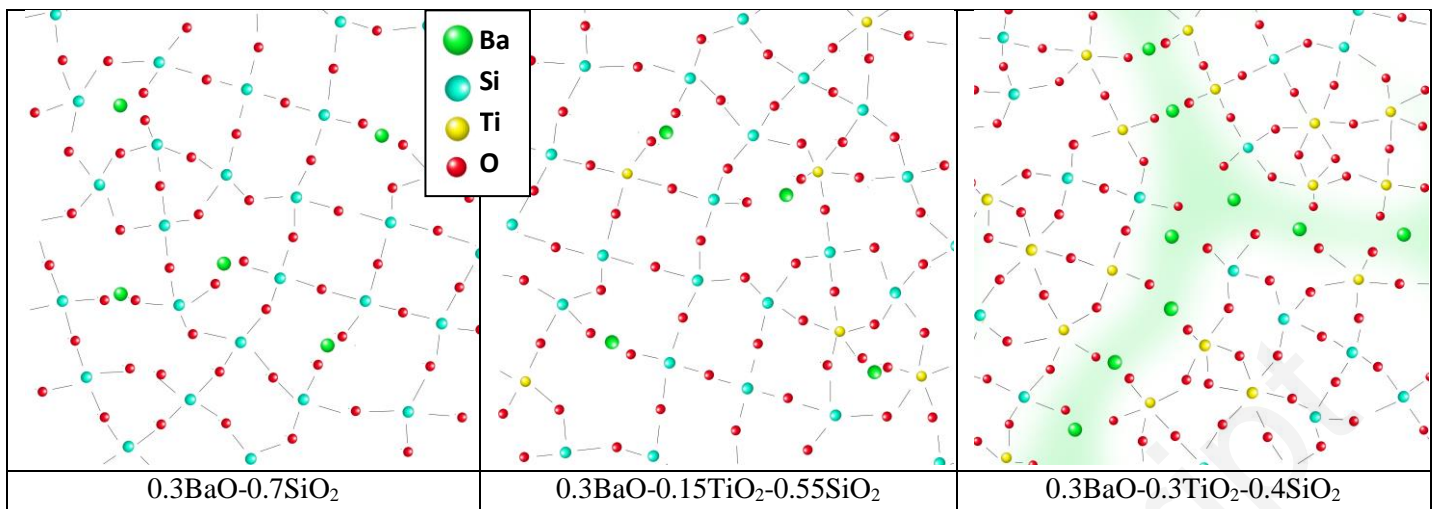


Fig. 4. Schematic drawings of the atomic network for  $x = 0; 0.15; 0.30$  glasses.

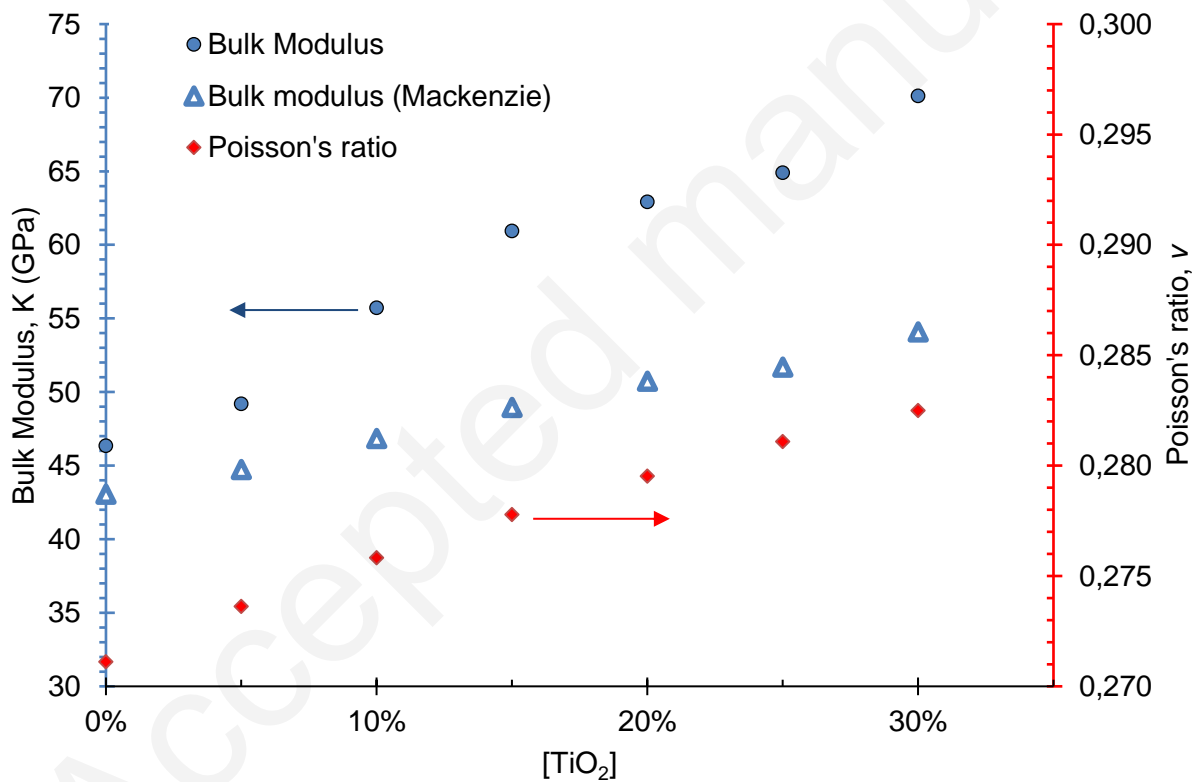


Fig. 5. Bulk modulus from experimental (USE) and Makishima and Mackenzie's model [28], and Poisson's ratio at room temperature, as a function of  $x = [TiO_2]$ .

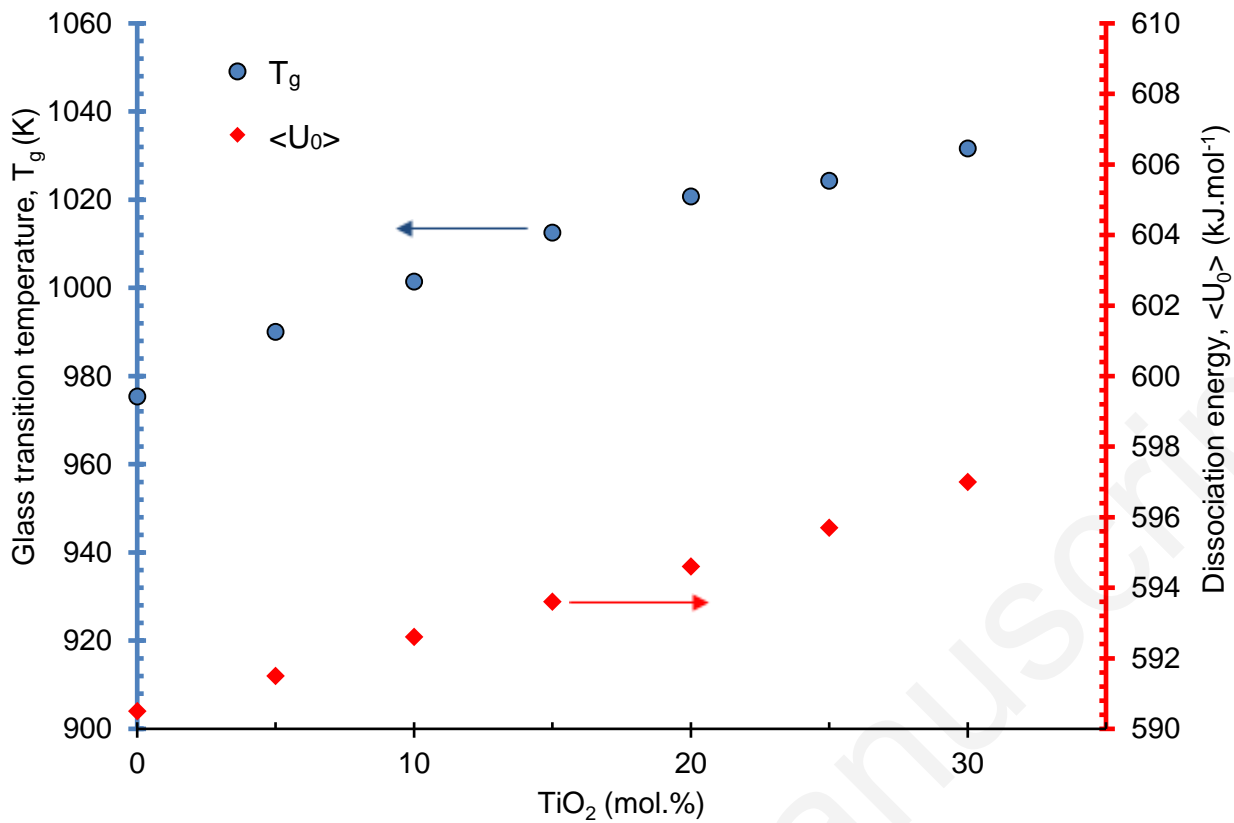


Fig. 6. Glass transition temperature obtained from viscosity measurements and dissociation enthalpy, calculated from Eq. (10) as a function of  $x = [TiO_2]$ .

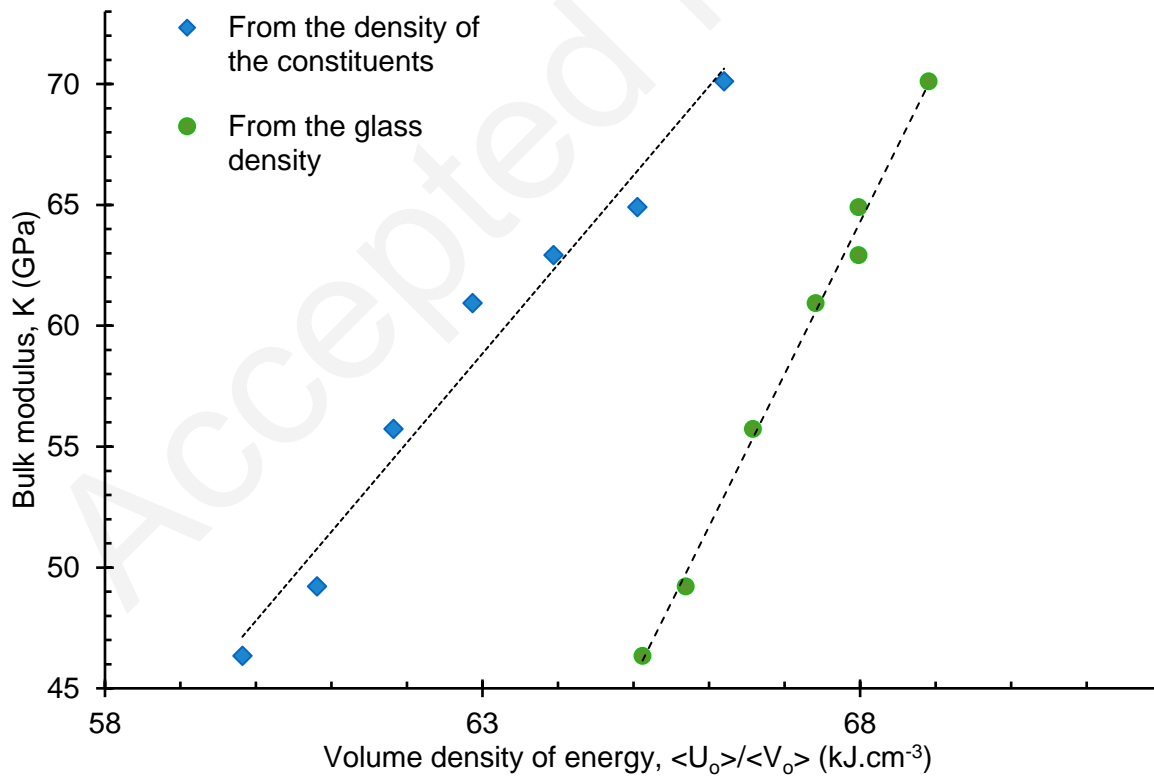


Fig. 7. Volume density of energy calculated from the density of each constituent Eq. (12) and from the density of the glass Eq. (10) versus the bulk modulus obtained via USE.

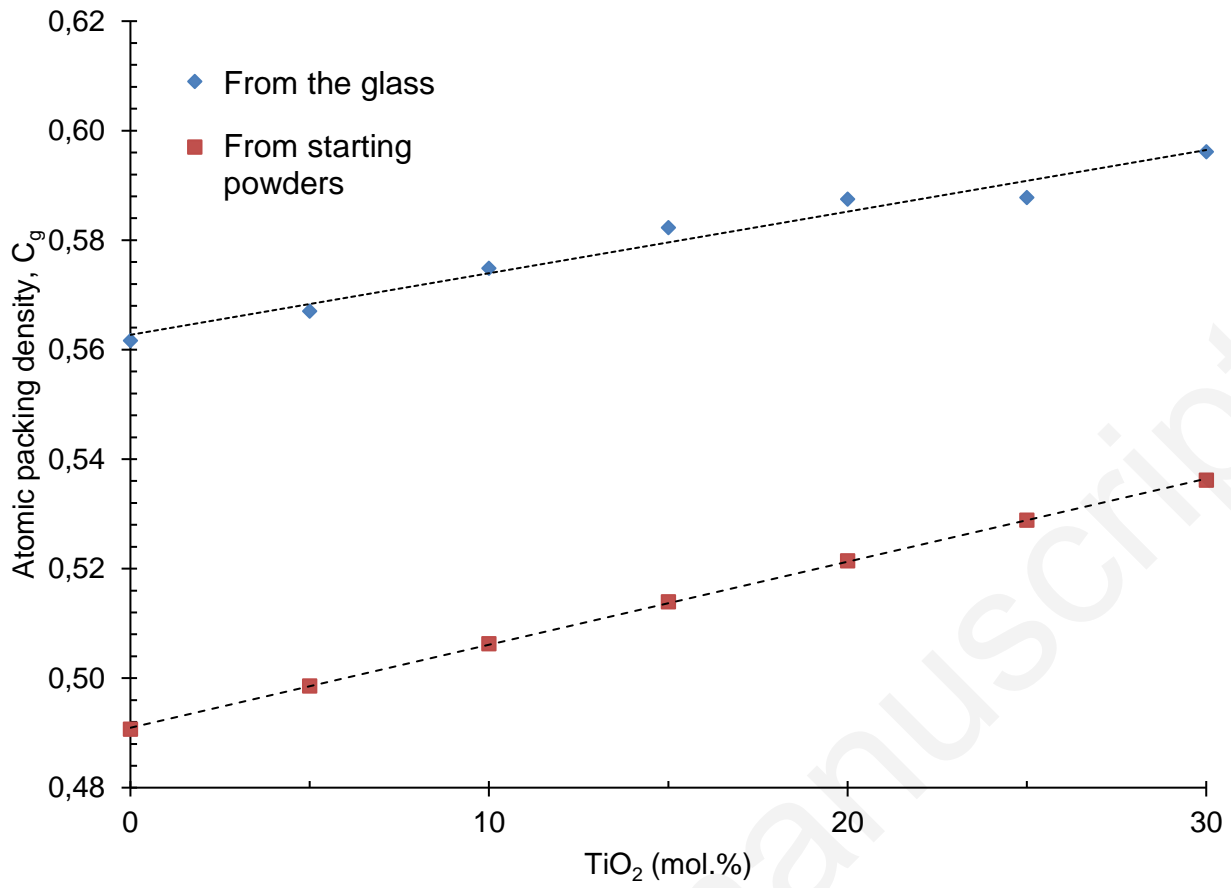


Fig.8. Atomic packing density calculated from the density of the glass Eq. (13) and the density of the starting powders as a function of TiO<sub>2</sub> molar content.

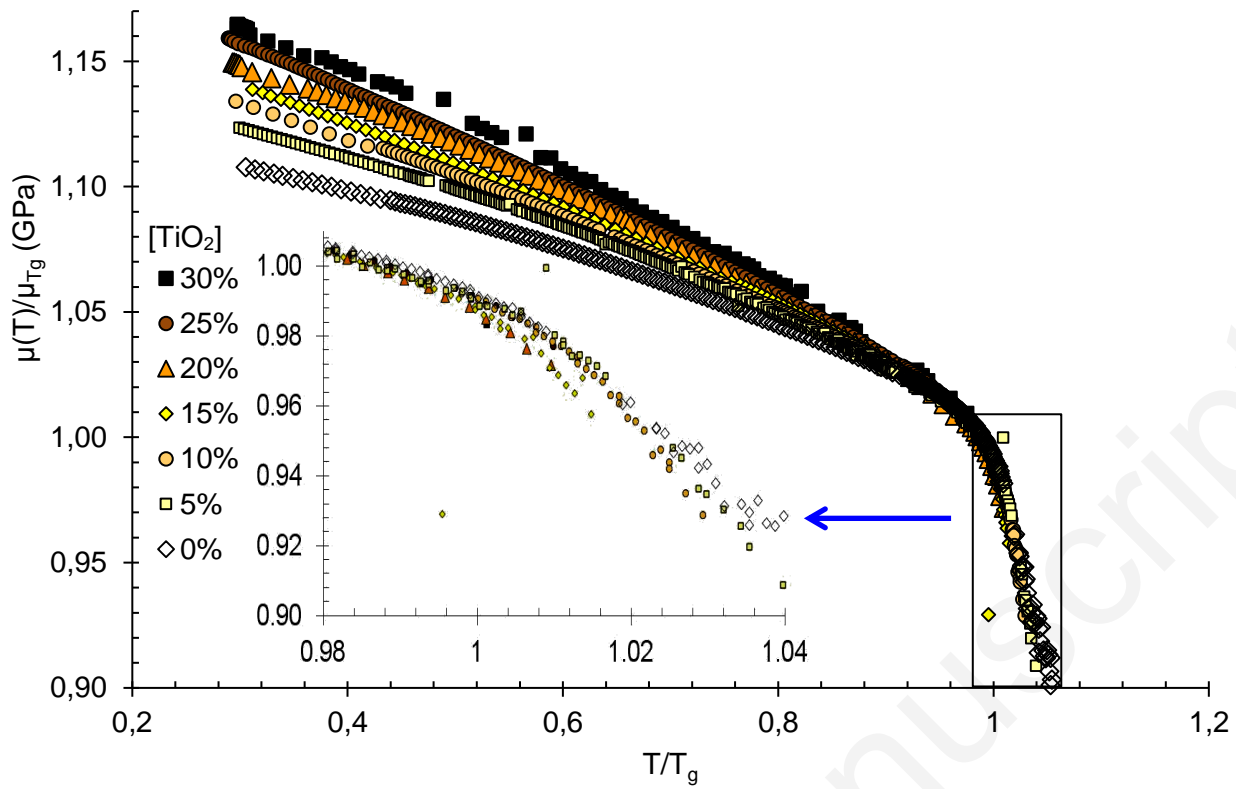


Fig. 9.  $\mu/\mu_{T_g}$  with temperature, obtained with RFDA measurements for all glasses.

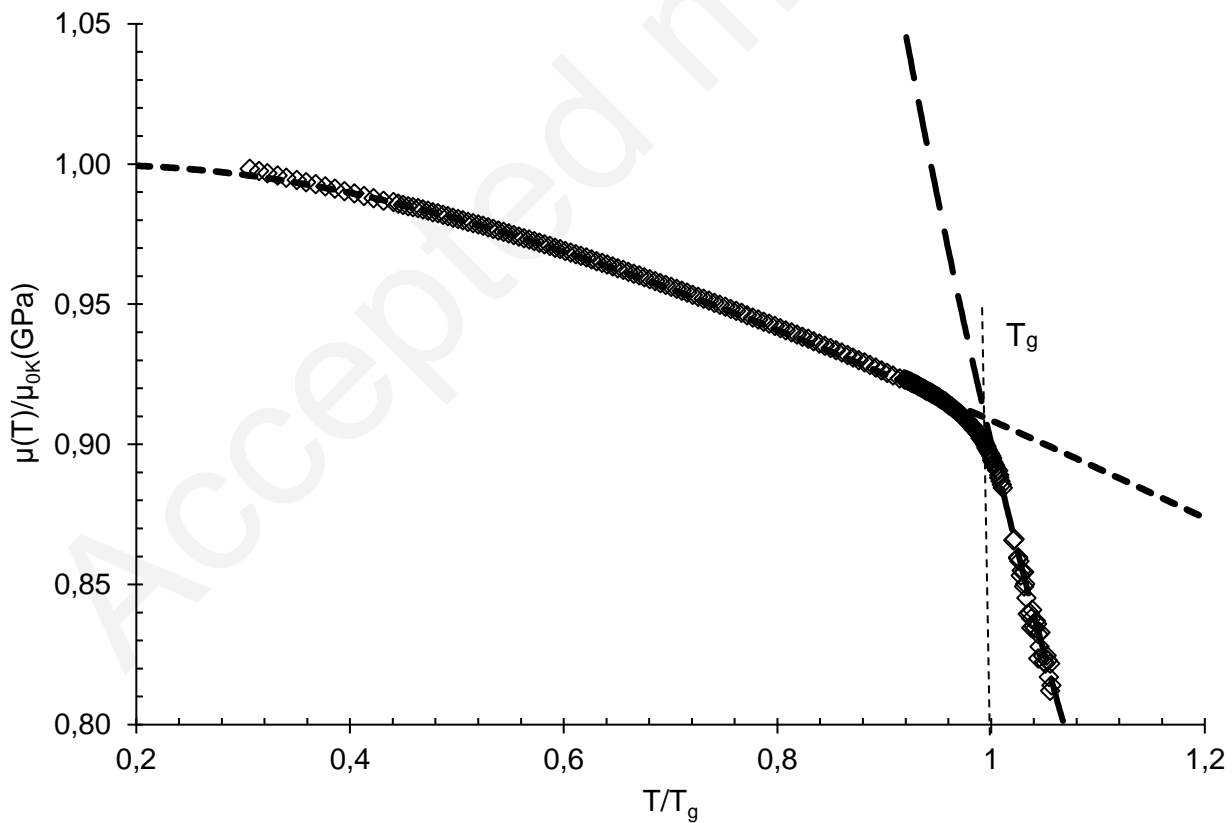


Fig. 10.  $\mu/\mu_{0K}$  versus  $T/T_g$  for  $0.3\text{BaO}-0.7\text{SiO}_2$ , fitting using Eq. (15) for  $T < T_g$  (dashed line) and Eq. (16) for  $T > T_g$  (dotted line).

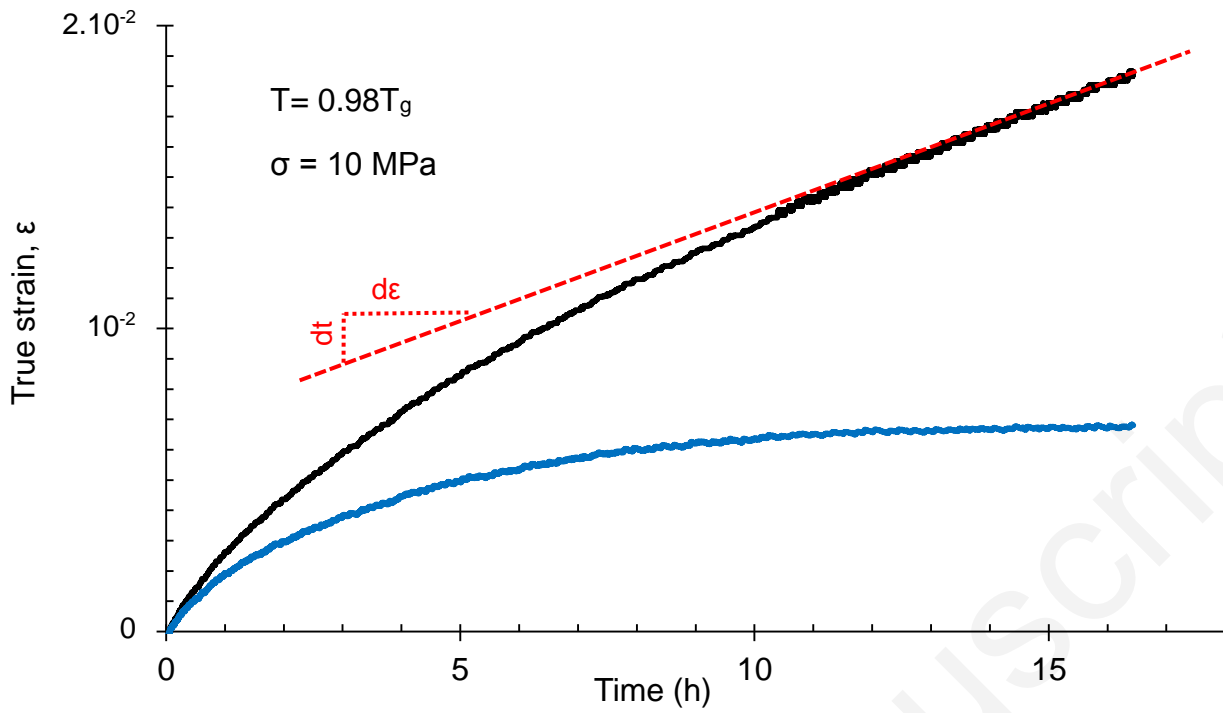


Fig. 11. Compressive creep experiment at  $0.98T_g$  under a 10 MPa load for the  $0.3\text{BaO}-0.2\text{TiO}_2-0.5\text{SiO}_2$  glass composition. The true strain (black) is the sum of the anelastic (or delayed elastic) (blue) and the stationary (viscous) (red) contributions.

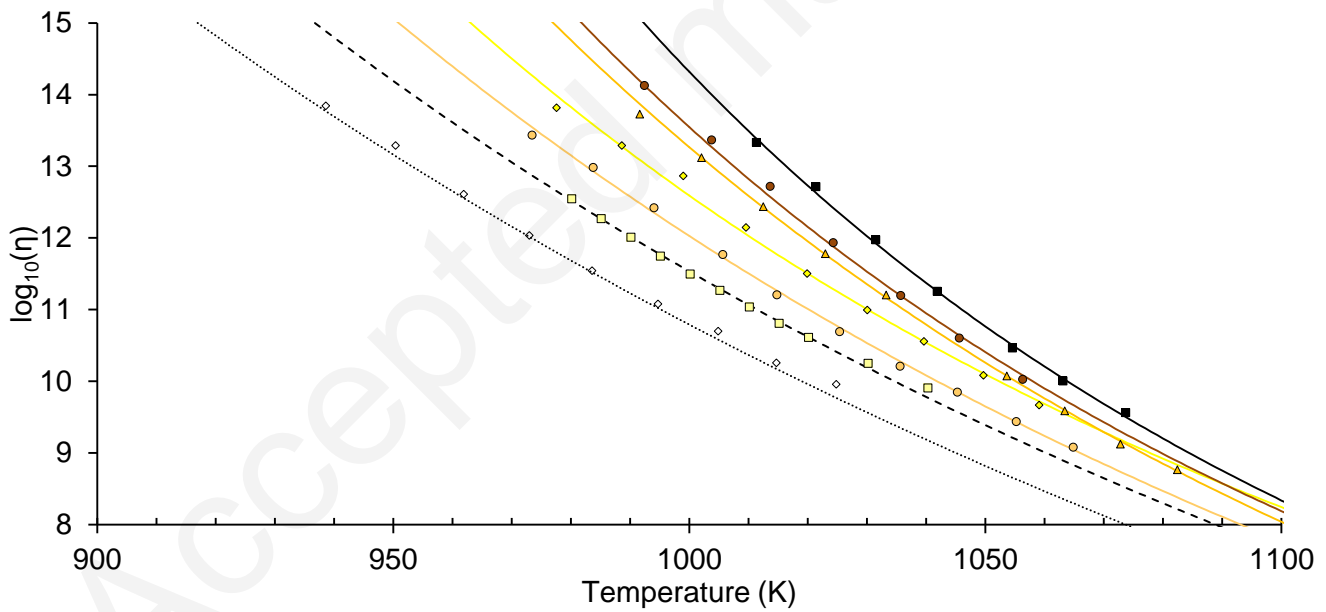


Fig. 12. Shear viscosity coefficient as a function of temperature. Lines show the modeling by means of Eq. (22).

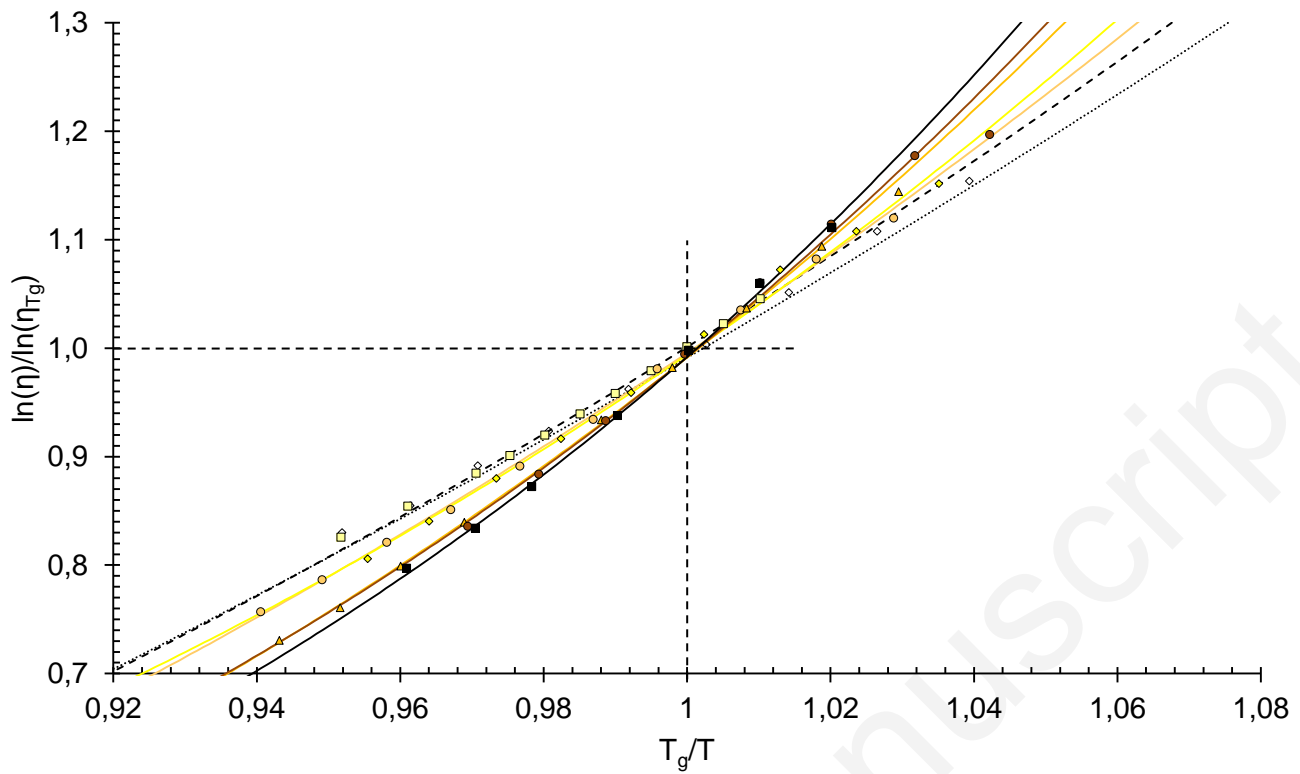


Fig. 13. Temperature dependence of the shear viscosity coefficient. Experimental data could be smoothly fitted by means of Eq. (22).

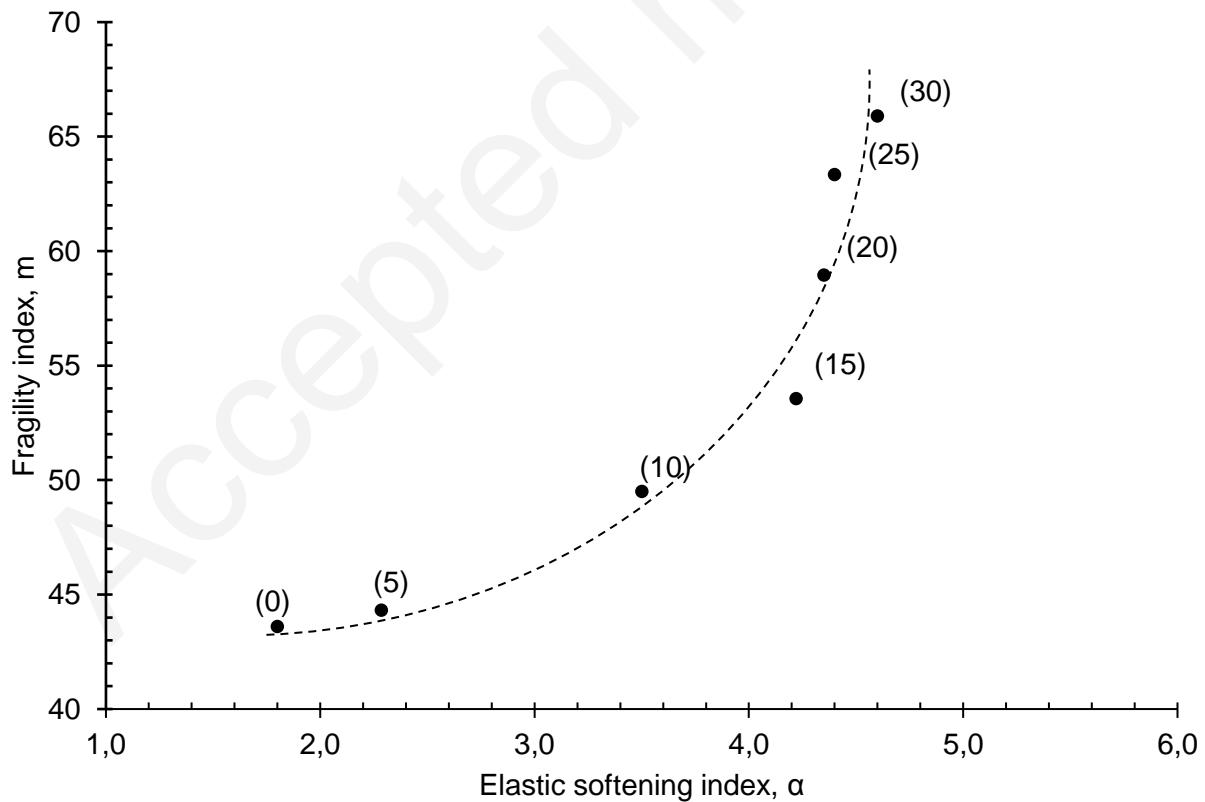


Fig. 14. Fragility index,  $m$ , calculated by means of Eq. (23) as a function of the elastic softening index,  $\alpha$ , calculated from Eq. (16) (numbers in brackets indicate the  $\text{TiO}_2$  content, in mol.%).